Electrical and magnetic properties of $La_{0.7-x}Y_xSr_{0.3}MnO_3$ $(0 \leqslant x \leqslant 0.20)$ perovskite at low temperature

1998 J. Phys.: Condens. Matter 10 9799

(http://iopscience.iop.org/0953-8984/10/43/024)

J. Phys.: Condens. Matter **10** (1998) 9799–9811. Printed in the UK PII: S0953-8984(98)91974-9

Electrical and magnetic properties of $La_{0.7-x}Y_xSr_{0.3}MnO_3$ ($0 \leqslant x \leqslant 0.20$) perovskite at low temperature

A Barman, M Ghosh, S Biswas, S K De and S Chatterjee

Department of Materials Science, Indian Association for the Cultivation of Science, Jadavpur, Calcuttta 700 032, India

Received 23 February 1998, in final form 30 July 1998

Abstract. Electrical and magnetic properties of $La_{0.7-x}Y_xSr_{0.3}MnO_3$ ($0 \leqslant x \leqslant 0.2$) have been extensively investigated at low temperature down to 1.8 K. The irreversibility of magnetic susceptibility between zero field cooling and field cooling increases with increasing Y content. The metal–insulator transition temperature (T_M) shifts towards lower temperature and the peak resistivity and magnetoresistance increase with the increase of x. Electrical conduction above T_M is dominated by the variable range hopping mechanism. The increase in resistivity at low temperature has been interpreted in terms of electron–electron interaction. The enhancement of magnetoresistance with the increase of Y content is due to the reduction in Mn–O–Mn bond angle and the mobility of charge carriers.

1. Introduction

The perovskites of the form $(La, A)MnO_3$ (A is a divalent ion such as Ca, Sr, Ba) have become a fascinating system for recent researchers due to their novel electrical and magnetic properties and also their potential application in the field of magnetic recording devices and magnetic field sensors [1–7]. Among these materials, the La–Ca–Mn–O and La–Sr–Mn–O systems have been explored mostly due to its giant magnetoresistive (GMR) property and occurrence of metal–insulator (M–I) transition at a temperature very near to the ferromagnetic transition (FM) temperature. The simultaneous appearance of the ferromagnetism and metallic state can be explained by the double exchange (DE) interaction [8, 9]. The strong on site exchange interaction between the doped carriers and the local spins, both of which are mainly composed of the Mn 3d orbital split by the ligand field, is responsible for these phenomena. The experimental studies such as a giant oxygen-isotope shift of the ferromagnetic transition temperature T_C [10], phonon frequency hardening near T_C [11] and anomalous volume thermal expansion [12] indicate that there exists a strong coupling between charge and lattice in addition to the coupling between spin and charge. Millis *et al* [13] pointed out from the theoretical calculations that only DE phenomena cannot explain satisfactorily the GMR properties in the lightly doped $La_{1-x}Sr_xMnO_3$ system. They suggested that the lattice distortion arising from the strong Jahn–Teller effect plays an important role in $La_{1-x}Sr_xMnO_3$ compounds.

The magnetic and transport properties of the manganite perovskites are strongly dependent on the internal (chemical) pressure [14–21] and external pressure [22–24]. It has been seen recently that internal pressure produced by the partial replacement of La with

0953-8984/98/439799+13$19.50

the other trivalent rare earth or related atoms with smaller ionic radii causes a decrease of Curie temperature T_C, and a large enhancement of magnetoresistance (MR). The substitution of Y for La in $La_{0.7-x}Y_xCa_{0.3}MnO_3$ yields the largest enhancement in MR in comparison with other rare earth substitution [17, 20]. The external pressure however produces opposite effects, i.e., an increase of T_C and a decrease in MR as observed for $La_{1-x}Sr_xMnO_3$ systems. These effects have been discussed by many of the authors by variation of electronic band width, W, as a function of applied and chemical pressure, considering the influence of W on the Mn–O–Mn bond angle [14, 16].

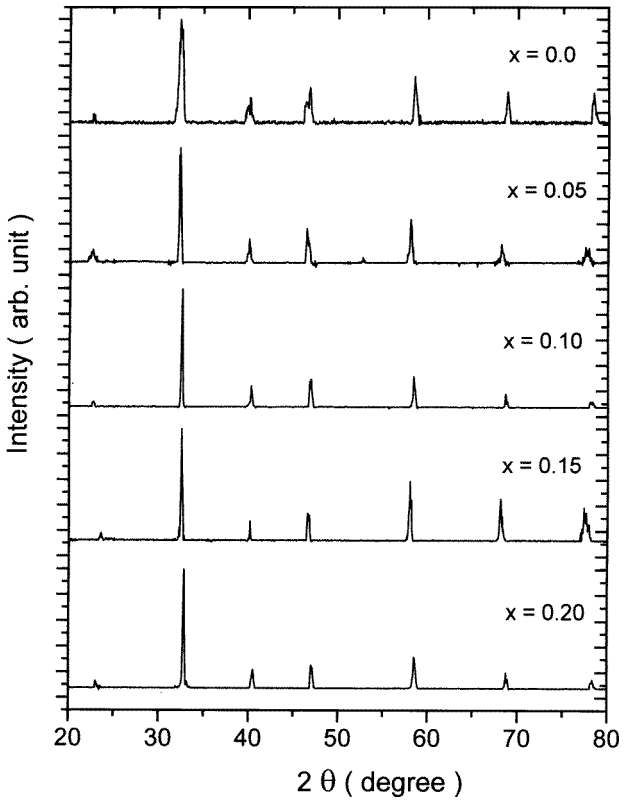

Figure 1. Intensity (in arbitrary units) is plotted against 2θ (in degrees) for the samples in the series $La_{0.7-x}Y_xSr_{0.3}MnO_3$ ($0 \leqslant x \leqslant 0.2$).

The electrical and magnetic properties of $La_{1-x}Sr_xMnO_3$ ($0 \leqslant x \leqslant 0.6$) single crystals have been investigated by Urushibara *et al* [6]. They observed that T_C increases monotonically from 145 to 371 K as the amount of Sr doping increases. The phase diagram of $La_{1-x}Sr_xMnO_3$ is different from that of $La_{1-x}Ca_xMnO_3$ due to the differences in radii of Sr and Ca ions. The Curie temperature of $La_{0.7}Sr_{0.3}MnO_3$ is 220 K, below room temperature, while that of $La_{0.7}Sr_{0.3}MnO_3$ is 369 K above room temperature. Thus the studies on the replacement of La by introducing the smaller ions like Y in Sr doped materials will be more interesting than Ca doped systems due to the fact that in the former case there is a possibility to obtain T_C and large MR near room temperature which has a great importance from the technological point of view. Moreover, to ascertain the possible origin of the unusual observations in the case of the partial replacement of La by a smaller rare earth at constant

doping concentration, more systematic studies are required. These stimulate us to study the electrical resistivity, magnetoresistance, dc magnetic susceptibility and magnetization of $La_{0.7-x}Y_xSr_{0.3}MnO_3$ ($0 \leqslant x \leqslant 0.2$) within a temperature range of 1.8–300 K and magnetic field range of 0–7 T.

2. Experiment

The samples in the series with nominal composition $La_{0.7-x}Y_xSr_{0.3}MnO_3$ ($0 \leqslant x \leqslant 0.2$) were prepared by conventional solid state reaction. Appropriate amounts of La_2O_3, Y_2O_3, $SrCO_3$ and $MnCO_3$ (all from Aldrich Chemical Ltd and 99.9% purity) were taken, maintaining the required stoichiometric ratio, and mixed very well with distilled ethanol to obtain a homogeneous mixture. The mixtures were then dried and calcined at 900 °C for 24 h. The calcined mixtures were then reground, pressed into pellets with pressure of about 4 tons cm^{-2} and sintered in open air at 1200 °C for 48 h. This process was repeated at least three times for each sample to obtain better homogeneity and better crystallinity. The samples were finally sintered at 1400 °C for 24 h. The XRD pattern of the samples with Cu Kα radiation has revealed the single phase perovskite structure of the samples with no significant trace of impurity as shown in figure 1. Circular disks of 12 mm diameter were obtained which were then cut into rectangular pieces of approximate dimension of about 10 mm × 2 mm × 1 mm for resistivity measurement. Four leads were made on the samples by ultrasonic soldering on which copper wires of about 100 μm diameters were connected. The linear current–voltage relationships at several fixed temperatures have confirmed the ohmic contact for the electrical measurement. The resistivity and magnetoresistance were measured by the standard four probe technique within a temperature region of 1.8 K to 300 K and a magnetic field region of 0 to 7 T in a He^4 cryostat (Oxford Instruments Ltd) equipped with an 8 T superconducting magnet. Magnetization and dc magnetic susceptibility were measured with the help of a SQUID magnetometer up to a field of 7 T.

3. Results and discussions

Figure 2(a) shows the temperature variation of dc magnetic susceptibility at 100 Oe, for zero field cooling (ZFC) and field cooling (FC). The susceptibility data at $H = 100$ Oe show the onset of irreversibility between the ZFC and FC curves for all the samples. The ZFC and the FC curves have started separating at about 320, 270, 220, 180 and 160 K for the samples with $x = 0.0$, 0.05, 0.10, 0.15 and 0.20 respectively. While the ZFC curves started decreasing towards lower temperature after showing a maximum, the FC curves continued to increase and finally tend to saturate down to the lowest temperature measured. The ratios of χ_{FC}/χ_{ZFC} at 5 K for $H = 100$ Oe are nearly 1.15, 1.29, 1.40, 1.42 and 1.60 for the samples with $x = 0.0$, 0.05, 0.10, 0.15 and 0.20 respectively. Thus we see that this irreversibility is increasing with increase in Y content, i.e., with decrease in average ionic radius at the A site, $\langle r_A \rangle$. Such behaviour has already been observed in several manganate systems and it has been suggested that this irreversibility arises possibly due to the canted nature of the spins or due to the random freezing of spins [14, 25, 26]. However as H increases this irreversibility starts to diminish very rapidly and it almost disappears above $H = 200$ Oe. This implies that the anisotropy field is not very large. All the samples have shown a transition from the ferromagnetic to the paramagnetic state.

The magnetization as a function of applied magnetic field at various temperatures for $x = 0.05$ is shown in figure 2(b). The magnetic transition temperature T_C which is

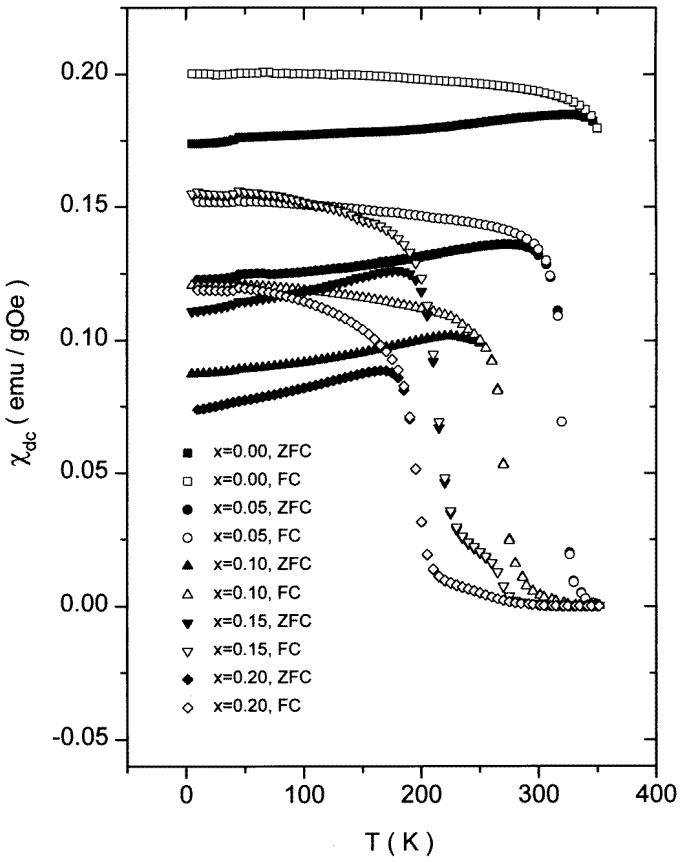

(a)

Figure 2. (a) DC magnetic susceptibility (χ_{dc} (emu g^{-1} Oe^{-1})) is plotted against temperature (T(K)) for the samples in the series $La_{0.7-x}Y_xSr_{0.3}MnO_3$ ($0 \leqslant x \leqslant 0.2$) for zero field cooling (ZFC), warmed in $H = 100$ Oe and field cooling (FC) in $H = 100$ Oe, on warming. (b) DC magnetization (M(emu g^{-1})) is plotted against magnetic field (H(T)) for the sample $La_{0.65}Y_{0.05}Sr_{0.3}MnO_3$ at several fixed temperatures.

the conventional Curie temperature is 325, 275, 225, 180 and 165 K and the saturation magnetization is 92.5, 91.7, 91, 89 and 87 emu g^{-1} for $x = 0.0$, 0.05, 0.10, 0.15 and 0.20 respectively. Hence both the Curie temperature and saturation magnetization decrease with the increase of Y doping. This indicates that the magnetic exchange interaction decreases with decrease of $\langle r_A \rangle$.

The zero field temperature dependence of resistivity of the samples normalized to resistivity at room temperature (300 K) is shown in figure 3. A large resistivity peak appears for almost all the samples at low temperature. However, the sample with $x = 0$ does not show any peak up to $T = 300$ K, although a trend towards a peak appears. The previously reported data show a resistivity peak well above 300 K for this sample [5, 6]. The temperature T_M at which the resistivity maximum occurs decreases systematically with the increasing Y doping. The peak corresponds to a metal–insulator transition which is clear from the behaviour of the resistivity data above and below T_M.

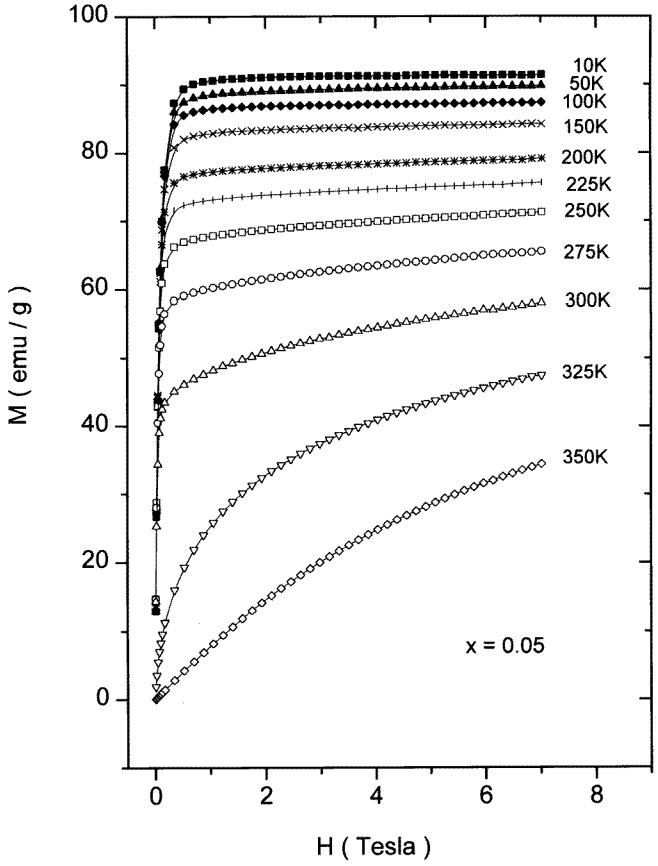

(b)

Figure 2. (Continued)

Firstly we focus our attention to the low temperature region. The resistivity for all the samples decreases with increase in temperature and then shows a minimum after which it increases with increase in temperature. The minimum occurs at $T = 30$ K for $x = 0.0$, $T = 32.5$ K for $x = 0.05$, $T = 35$ K for $x = 0.10$, $T = 38$ K for $x = 0.15$ and $T = 42$ K for $x = 0.20$. The minimum occurs in the metallic state and it has also been observed by previous workers [6]. However, not much attention was given to this region. The temperature dependence of resistivity for the disordered metallic materials can be described by the electron–electron interaction [27]. Hence we have tried to fit the temperature dependence of conductivity in this region with the formula $\sigma(T) = \sigma(0)+AT^{1/2}$ for the electron–electron interaction. A good fit is obtained for all the samples which is clear from figure 4. The temperature up to which the expression is valid is $T = 27$ K for $x = 0.0$, $T = 29$ K for $x = 0.05$, $T = 30$ K for $x = 0.10$, $T = 34$ K for $x = 0.15$ and $T = 36$ K for $x = 0.20$. The disorder increases in the system upon random substitution of Y ions in place of La ions. This plays an important role in bringing the electron–electron interaction as a quantum correction in the resistivity behaviour at low temperature.

The resistivity below T_M, that is in the ferromagnetic regime, shows a metallic behaviour where it increases with increase in temperature. We have fitted the temperature dependence

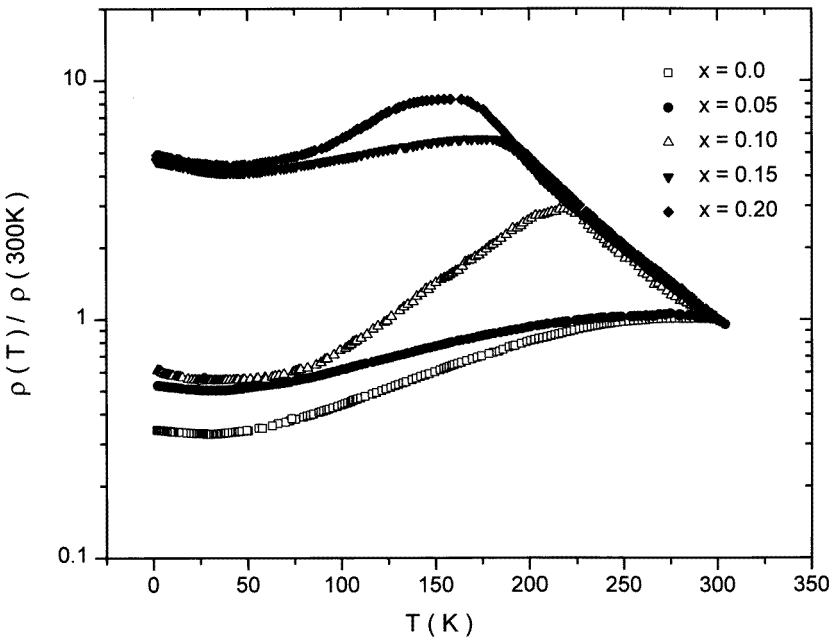

Figure 3. Temperature (T(K)) variation of resistivity normalized to resistivity at 300 K ($\rho(T)/\rho(300\ \mathrm{K})$) is plotted for the samples in the series $La_{0.7-x}Y_xSr_{0.3}MnO_3$ ($0 \leqslant x \leqslant 0.2$).

of resistivity behaviour in this region with the formula $\rho(T) = \rho(0) + AT^2$. Figure 5(a) shows a good fit for all the samples up to a temperature just below T_M. This result suggests that the electron–electron scattering process associated with spin fluctuation plays an important role in these materials [6, 28, 29]. The value of the coefficient A obtained from the fitting has shown a very good correlation with $\rho(T_M)$ which is clear from figure 5(b), where $\rho(T_M)$ and A both are plotted as a function of $\langle r_A \rangle$, the average ionic radius at the A site of the perovskite ABO_3. A strong electron correlation is evident from this result which remains active even up to the temperature range in the vicinity of T_M. The resistivity has started to rise steeply and deviates from the T^2 behaviour while approaching T_M. This should be associated with some static or dynamic distortion and may be both of the corner shared MnO_6 octahedra in these perovskites [8, 9, 30].

The resistivity above T_M is of semiconducting nature, that is, it decreases with increase in temperature. From figure 3 it is clear that at $T > T_M$, the functional dependence of $\rho(T, 0)$ is identical for all the samples. We have tried to fit the resistivity data above T_M with the formula $\rho = \rho_0 \exp[T_0/T]^{1/4}$ for the variable range hopping between localized states [31]. A good fit is obtained for all the samples with T_0 increasing systematically with Y doping as depicted in figure 6. Figures 7(a) and 7(b) show the systematic changes of T_0, T_M and $-$MR% in terms of $\langle r_A \rangle$ and reveal that T_M decreases and both T_0 and MR increase with decrease in $\langle r_A \rangle$. The large enhancement of $\Delta\rho(T)/\rho$ (defined as $[\rho(T_M) - \rho(300\ \mathrm{K})/\rho(300\ \mathrm{K})]$, which is clear from figure 3, appear to originate from the occurrence of T_M at a lower temperature and simultaneous enhancement of the T_0 value. The parameter T_0 is related to the spatial extension (L_{loc}) of the localized states and to the density of states $N(E_F)$ at the Fermi level of the Mott relation [31], $T_0 = 16/K_B N(E_F) L_{loc}^3$ where K_B is the Boltzmann constant. The increase in $N(E_F)$ due to the decrease of bandwidth

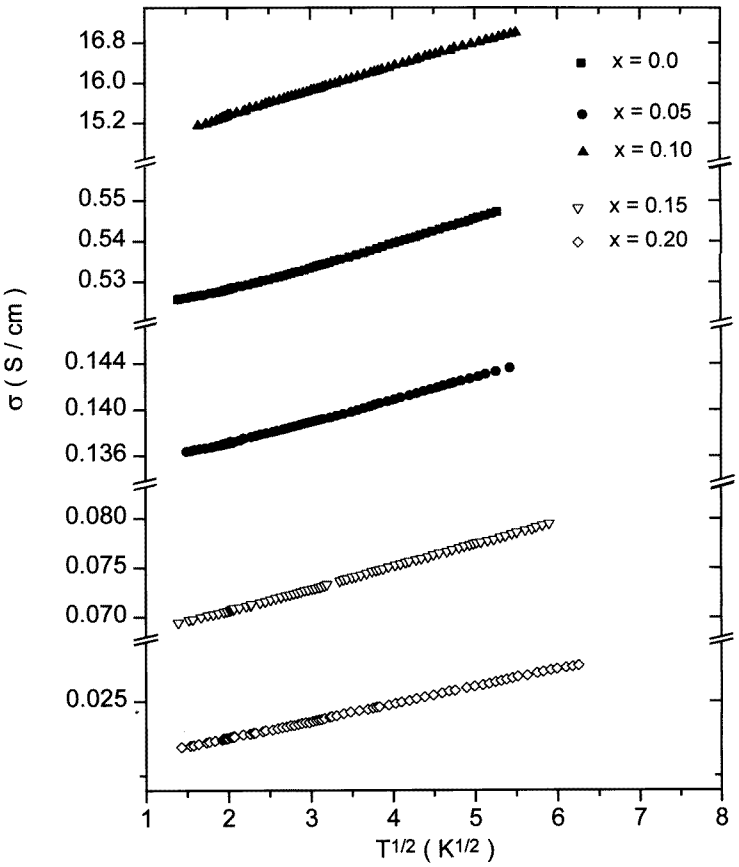

Figure 4. Conductivity (σ(S cm^{-1})) is plotted against $T^{1/2}$(K$^{1/2}$) for the samples, in the series $La_{0.7-x}Y_xSr_{0.3}MnO_3$ ($0 \leqslant x \leqslant 0.2$).

while $\langle r_A \rangle$ decreases indicates that the reduction of L_{loc} is the main factor determining the enhancement of T_0. Therefore it may be stated that decrease of the bandwidth associated with an increase of the lattice distortion decreases the localization length and consequently the carrier mobility is reduced.

Figure 8 shows the $-$MR% $[((\rho(H) - \rho(0))/\rho(0)) \times 100]$ as a function of temperature in the temperature range of 2 to 300 K at a fixed magnetic field of 7 T for all the samples. The maximum value of $-$MR% is found to be nearly 61% for the sample with $x = 0.2$, whereas for the sample with $x = 0.0$ it is nearly 38% [5]. The sample with $x = 0.0$ does not show any peak in the $-$MR% up to 300 K, but the four samples show prominent peaks in the $-$MR% in this temperature range. The sample with $x = 0.05$ shows the peak near 275 K, that with $x = 0.10$ shows the peak at about 225 K, the samples with $x = 0.15$ shows a peak at about 180 K and the sample with $x = 0.20$ shows a peak at about 165 K. The temperature corresponding to the peak values of magnetoresistance agrees very well with the T_M and T_C values and also decreases rapidly towards a lower temperature with increase in Y doping, that is with decrease in $\langle r_A \rangle$. On the other hand the maximum value of the magnetoresistance increases with decrease in $\langle r_A \rangle$. Figure 7(b) shows the variation of T_M and the maximum value of $-$MR% as a function of $\langle r_A \rangle$. A very good correlation is found

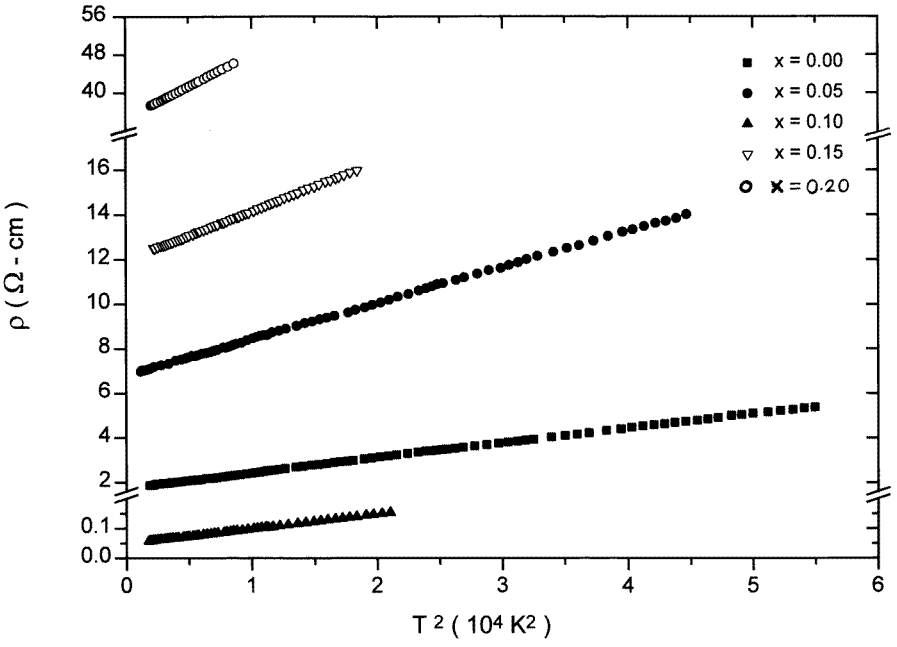

(a)

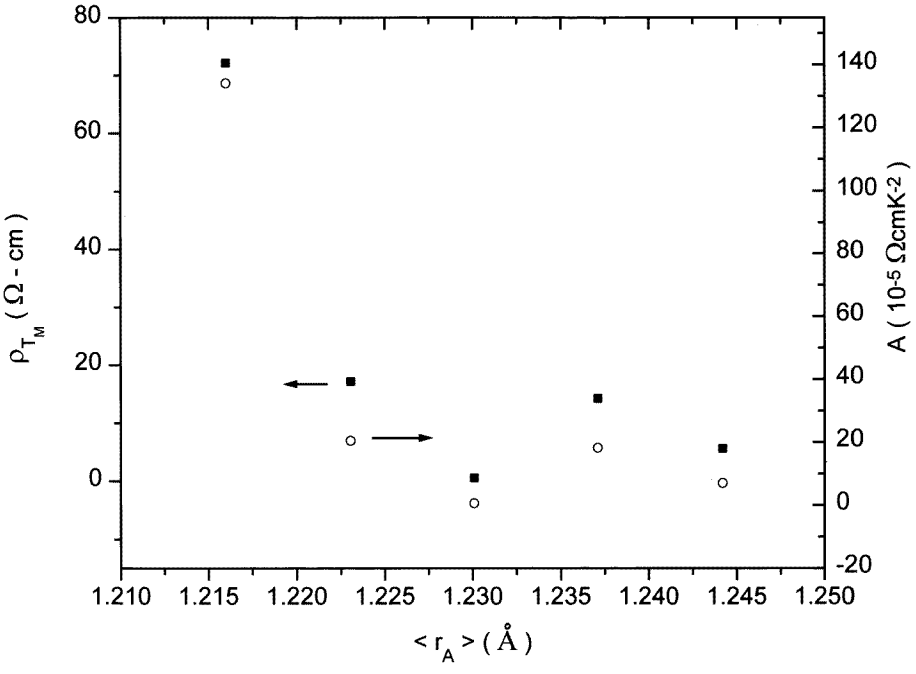

(b)

Figure 5. (a) Resistivity ($\rho(\Omega$ cm)) is plotted against $T^2(\mathrm{K}^2)$ for the samples in the series $La_{0.7-x}Y_xSr_{0.3}MnO_3$ ($0 \leqslant x \leqslant 0.2$) in the metallic region. (b) Peak value of resistivity (ρ_{T_M}) corresponding to the metal–insulator transition temperature (T_M) and the coefficient A obtained from the fitting with the formula $\rho(T) = \rho(0) + AT^2$ is plotted against $\langle r_A \rangle$, the average ionic radius at the A site for the samples in the series $La_{0.7-x}Y_xSr_{0.3}MnO_3$ ($0 \leqslant x \leqslant 0.2$).

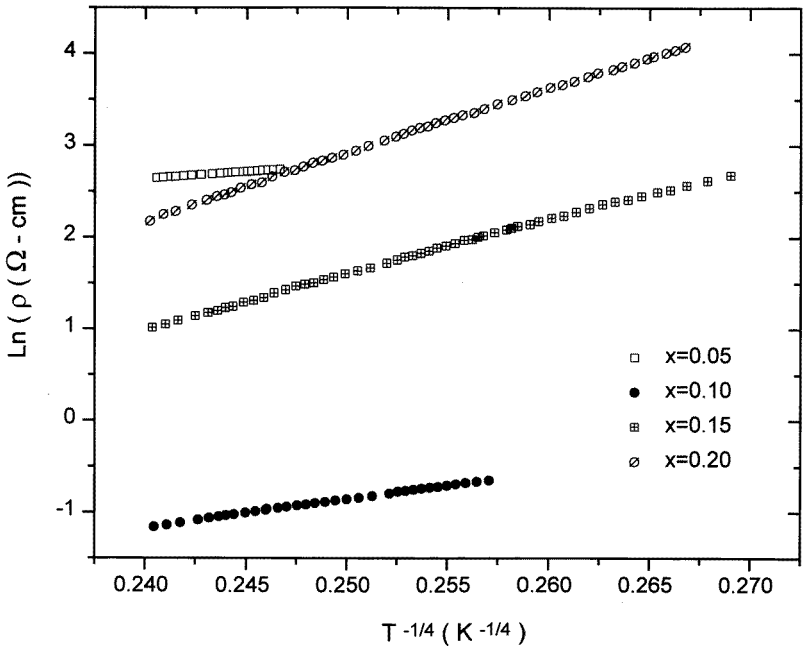

Figure 6. Logarithm of resistivity ($\ln\rho(\Omega$ cm)) is plotted against $T^{-1/4}(K^{-1/4})$ for the samples in the series $La_{0.7-x}Y_xSr_{0.3}MnO_3$ ($0.05 \leqslant x \leqslant 0.2$).

between the two which suggests that there is a close association between the reduction of T_M, enhancement of $\Delta\rho(T)/\rho$ and at the same time enhancement of $-$MR% with decrease in $\langle r_A\rangle$.

The magnetic and transport properties of $La_{0.7-x}Y_xSr_{0.3}MnO_3$ can be interpreted in terms of the ionic radii of La and Y ions. In general, the structural stability of a perovskite compound ABO_3 ($LaMnO_3$) is described by the tolerance factor $t = (r_A + r_O)/(r_B + r_O)\sqrt{2}$, where r_A, r_B and r_O are the ionic radii of A, B and oxygen respectively. For the ideal cubic perovskite structure, $t = 1$ and the regular BO_6 octahedra share the corners of the cubic unit cell to form a three dimensional array with the A ions. For the smaller values of $\langle r_A\rangle$, the structure becomes distorted as the BO_6 octahedra tilt and rotate in order to fill the extra space around A, to optimize the A–O bond length. The buckling of the MnO_6 octahedron causes the Mn–O–Mn bond angle θ to be less than its ideal value of 180°. The Mn–O–Mn bond angle determines the overlap of Mn (e_g) and O (2p) orbitals and hence plays an important role in the electronic and magnetic properties. The replacement of La by the smaller ion Y yields a decrease in θ and consequently weakens the double exchange interaction between Mn^{3+} and Mn^{4+} ions and also reduces the charge carrier band width. These effects will produce a decrease in T_M and increase in peak resistivity with the increase of amount of Y.

Figures 9(a) and (b) shows the magnetoresistance as a function of magnetic field at two fixed temperatures $T = 4.2$ K and $T = 10$ K respectively. The inset of figure 9(b) shows the magnetization against magnetic field at $T = 10$ K for some of the samples. The magnetoresistance at a fixed temperature increases systematically with increase in Y doping as a function of magnetic field. This was also found from the magnetoresistance–temperature curves at fixed magnetic field as shown in figure 8. From figure 9(b) it is clear that

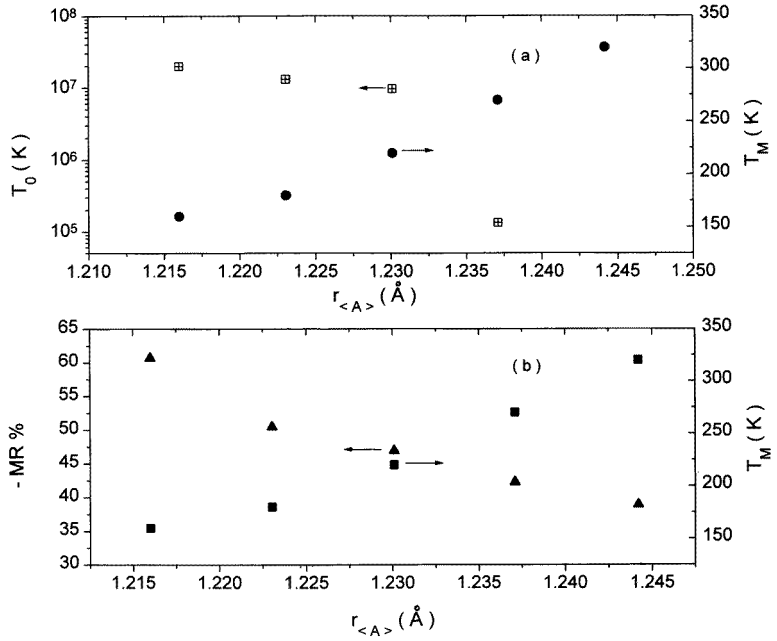

Figure 7. (a) The value of T_0 obtained from the fitting with the formula $\rho = \rho_0 \exp[T_0/T]^{1/4}$ and the temperature T_M corresponding to the metal–insulator transition are plotted against $\langle r_A \rangle$, the average ionic radius at the A site for the samples in the series $La_{0.7-x}Y_xSr_{0.3}MnO_3$ ($0 \leqslant x \leqslant 0.2$). (b) The peak value of negative magnetoresistance percentage ($-$MR%) at an applied magnetic field of 7 T and the temperature corresponding to the metal–insulator transition (T_M) are plotted against $\langle r_A \rangle$, the average ionic radius at the A site for the samples in the series $La_{0.7-x}Y_xSr_{0.3}MnO_3$ ($0 \leqslant x \leqslant 0.2$).

there is a strong correlation between the magnetization and magnetoresistance. Below the magnetic saturation field (H_s), the magnetoresistance drops rapidly with the increase of the field. However, above the saturation field magnetoresistance drops rather slowly but still a significant amount of change was observed. From the magnetoresistance–temperature plot as shown in figure 8, we see that there are two distinct regions. One region is prominent at the high temperature range, near the ferromagnetic transition temperature; the other is prominent at low temperature where a substantial amount of magnetization exists. We focus our attention on the low temperature magnetoresistance. The magnetoresistance changes very rapidly at the early small change in the magnetic field where the magnetization has not yet saturated and also changes very steeply. Above the saturation field, the magnetoresistance changes rather slowly with the magnetic field and the magnetization reflects the same behaviour. This result can be interpreted by the double exchange interaction between pairs of Mn^{3+} and Mn^{4+} ions. In this mechanism a parallel alignment of manganese spins is required for the electrons to be transferred between the ions to give higher electrical conductivity. The manganese ions are ferromagnetically ordered inside a single domain even at a temperature well below T_C and the transfer of electrons between pairs of Mn^{3+} and Mn^{4+} ions inside a single domain is easy. But for the unmagnetized sample there are a number of domains which have different magnetization directions. The pairs of spins of Mn^{3+} and Mn^{4+} ions near the domain wall boundary may not be parallel and as a result electron transfer between the Mn^{3+} and Mn^{4+} ions across the domain wall boundary is

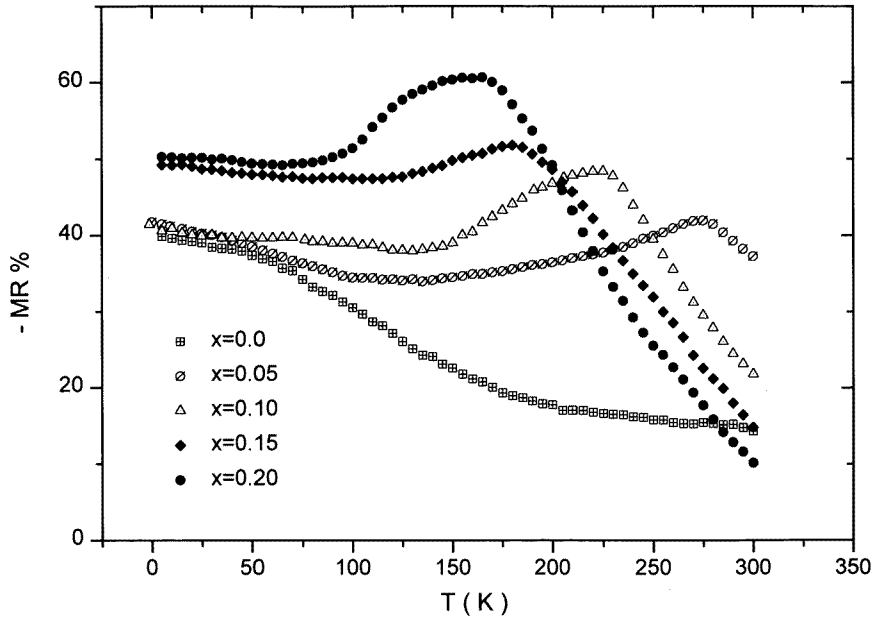

Figure 8. Negative magnetoresistance percentage (−MR%) at an applied magnetic field of 7 T is plotted against temperature (T(K)) for the samples in the series $La_{0.7-x}Y_xSr_{0.3}MnO_3$ ($0 \leqslant x \leqslant 0.2$).

difficult resulting in a high resistivity. Application of a strong enough magnetic field will tend to align the magnetic domains along its own direction. As a result the electron transfer across the domain wall boundary become easier and resistivity decreases giving a large change in the magnetoresistance in this range of magnetic field. Above the saturation field there are still small cantings of the manganese moments inside each single domain and as a result magnetization increases slowly with magnetic field even at $H \gg H_s$. For $H > H_s$ the canting angle between the manganese moments inside each single domain becomes smaller and therefore electrons will transfer more easily between pairs of Mn^{3+} and Mn^{4+} ions giving a further decrease in the resistivity and change in the magnetoresistance. This may be the possible explanation for the magnetoresistance behaviour well below T_C [32].

4. Conclusions

We have studied the effect of Y substitution for La on the temperature dependence of resistivity, magnetoresistivity and magnetic properties for a fixed doping concentration in the $La_{0.7}Sr_{0.3}MnO_3$ compound. The small anisotropic field and the reduced magnetization with the increase of Y content indicate that the irreversibility in magnetic susceptibility may be due to the canted arrangement of spins. The replacement of La by Y in $La_{0.7}Sr_{0.3}MnO_3$ leads to a decrease in Curie temperature and an increase of peak resistivity and magnetoresistance. Such behaviours are qualitatively explained in terms of the decrease in Mn–O–Mn bond angle and one electron bandwidth. The novel observation at low temperature of the upturn in resistivity with lowering temperature has been analysed in terms of quantum effects such as electron–electron interaction.

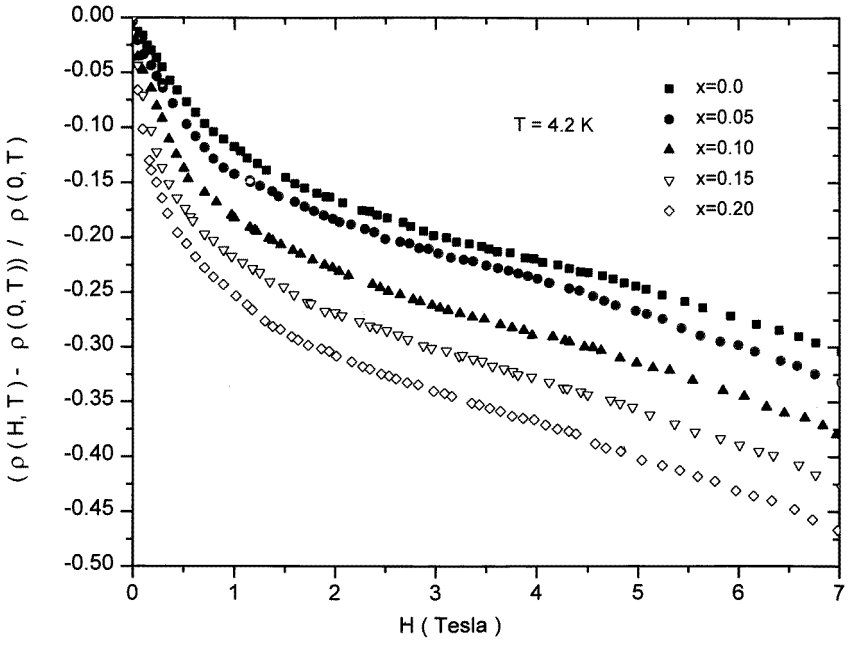

(a)

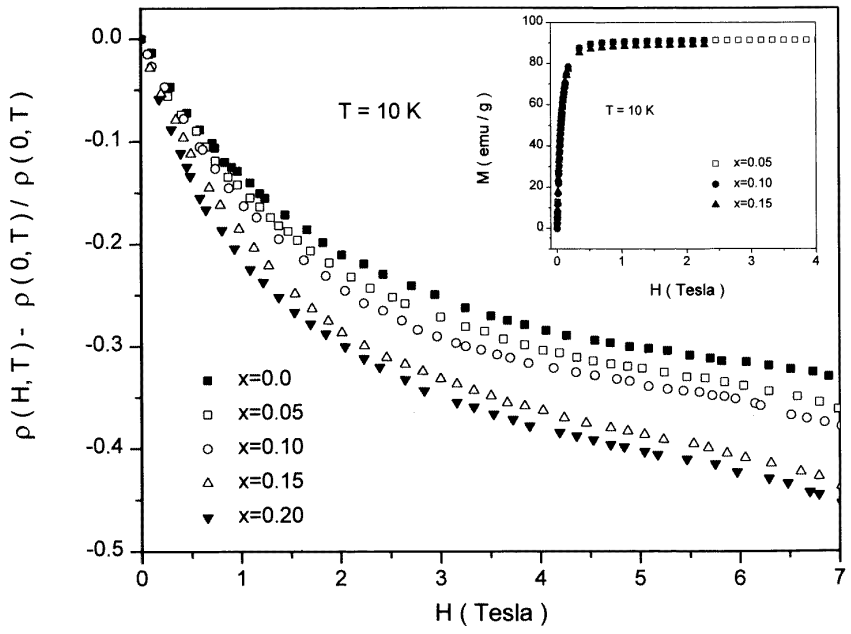

(b)

Figure 9. (a) Magnetoresistance $(\rho(H,T)-\rho(0,T))/\rho(0,T))$ is plotted against magnetic field (H(T)) at $T = 4.2$ K for the samples in the series $La_{0.7-x}Y_xSr_{0.3}MnO_3$ ($0 \leqslant x \leqslant 0.2$). (b) Magnetoresistance $((\rho(H,T)-\rho(0,T))/\rho(0,T))$ is plotted against magnetic field (H(T)) at $T = 10$ K for the samples in the series $La_{0.7-x}Y_xSr_{0.3}MnO_3$ ($0 \leqslant x \leqslant 0.2$). The inset shows the magnetization (M(emu g^{-1})) against magnetic field (H(T)) plot at $T = 10$ K for the samples with $x = 0.05$, 0.10, 0.15.

Acknowledgments

The experiment was performed under the financial support of the Department of Science and Technology, Government of India. One of the authors (M Ghosh) gratefully acknowledges UGC for a senior research fellowship. We are also indebted to Professor T K Bose and Dr M Foldeaki, Institut de Recherche sur l'Hydrogene, Department de Physique, Universite du Quebec a Trois-Rivieres, Quebec, Canada for magnetic measurements.

References

[1] von Helmolt R, Wecker J, Holzapfel B, Schultz L and Samwer K 1993 *Phys. Rev. Lett.* **71** 2331
[2] Jin S, Tiefel T H, McCormack M, Fastnacht R A, Ramesh R and Chen L H 1994 *Science* **262** 413
[3] Tomioka Y, Asamitsu A, Moritomo Y, Kuwahara H and Tokura Y 1995 *Phys. Rev. Lett.* **74** 5108
[4] von Helmolt R, Wecker J, Samwer K, Haupt L and Barner K 1994 *J. Appl. Phys.* **76** 6925
[5] Mahesh R, Mahendiran R, Raychaudhuri A K and Rao C N R 1995 *J. Solid State Chem.* **114** 297
[6] Urushibara A, Moritomo Y, Arima T, Asamitsu A, Kido G and Tokura Y 1995 *Phys. Rev.* B **51** 14 103
[7] Ramirez A P 1997 *J. Phys.: Condens. Matter* **9** 8171
[8] Zener C 1951 *Phys. Rev.* **82** 403
[9] Anderson P W and Hasegawa H 1955 *Phys. Rev.* **100** 675
de Gennes P G 1960 *Phys. Rev.* **118** 141
[10] Zhao G, Conder K, Keller H and Muller K A 1996 *Nature* **381** 676
[11] Kim K H, Gu J Y, Choi H S, Park G W and Noh T W 1996 *Phys. Rev. Lett.* **77** 1877
[12] De Teresa J M, Ibarra M R, Blasco J, Garcia J, Marquina C, Algarabel P A, Arnold Z, Kamenev K, Ritter C and von Helmolt R 1996 *Phys. Rev.* B **54** 1187
[13] Millis A J, Littlewood P B and Shraiman B I 1995 *Phys. Rev. Lett.* **74** 5144
Millis A J, Shraiman B I and Mueller R 1996 *Phys. Rev. Lett.* **77** 175
[14] Hwang H Y, Cheong S-W, Radaelli P G, Marezio M and Batlogg B 1995 *Phys. Rev. Lett.* **75** 914
[15] Hwang H Y, Palstra T T, Cheong S W and Batlogg B 1995 *Phys. Rev.* B **52** 15 046
[16] Foncuberta J, Martinez B, Seffar A, Pinol S, Garcia-Munoz J L and Obradors X 1996 *Phys. Rev. Lett.* **76** 1122
[17] Maignan A, Simon C, Caignaert V and Raveau B 1996 *J. Appl. Phys.* **79** 7891
[18] Guo Z B, Zhang N, Ding W P, Yang W, Zhang J R and Du Y W 1996 *Solid State Commun.* **100** 769
[19] Sun J R, Rao G H and Liang J K 1997 *Appl. Phys. Lett.* **70** 1900
[20] Jin S, O'Bryon H M, Tiefel T H, McCormack M and Rhodes W W 1995 *Appl. Phys. Lett.* **66** 382
[21] Blasco J, Garcia J, de Teresa J M, Ibara M R, Algarabel P A and Marquina C 1996 *J. Phys.: Condens. Matter* **8** 7427
[22] Neumeier J J, Hundley M F, Thompson J D and Heffner R H 1995 *Phys. Rev.* B **52** R7006
[23] Moritomo Y, Asamitsu A and Tokura Y 1995 *Phys. Rev.* B **51** 16 491
[24] Itoh M, Nishi K, Ding Yu J and Inaguma Y 1997 *Phys. Rev.* B **55** 14 408
[25] Arulraj A, Gundakaram R, Biswas A, Gayathri N, Raychaudhuri A K and Rao C N R 1998 *J. Phys.: Condens. Matter* **10** 4447
[26] Vogt T, Cheetham A K, Mahendiran R, Raychaudhuri A K, Mahesh R and Rao C N R 1996 *Phys. Rev.* B **54** 15 303
[27] Lee P A and Ramakrishnan T V 1995 *Rev. Mod. Phys.* **57** 287
[28] Kohno H and Yamada K 1991 *Prog. Theor. Phys.* **85** 13
[29] Guo Z, Zhang J, Zhang N, Ding W, Huang H and Du Y 1997 *Appl. Phys. Lett.* **70** 1897
[30] Radaelli P G, Marezio M, Hwang H Y, Cheong S-W and Batlogg B 1996 *Phys. Rev.* B **54** 8992
[31] Mott N F and Davis E A 1979 *Electronic Processes in Non-crystalline Materials* (Oxford: Clarendon)
[32] Ju H L, Gopalakrishnan J, Peng J L, Li Qi, Xiong G C, Venkatesan T and Greene R L 1995 *Phys. Rev.* B **51** 6143